POLISH POLAR RESEARCH
vol. 40, no. 3, pp. 205–225, 2019 doi: 10.24425/ppr.2019.129671

Sea ice regime in the Kara Sea during 2003–2017 based on high-resolution satellite data

Chenglin DUAN[1,2], Sheng DONG[1,2] and Zhifeng WANG[1,2*]

[1] *College of Engineering, Ocean University of China, Qingdao 266100, China*

[2] *Shandong Provincial Key Laboratory of Ocean Engineering, Qingdao 266100, China*

[*] *corresponding author <wzf1984@ouc.edu.cn>*

Abstract: In this paper, the recent ice regime variations in the Kara Sea have been described and quantified based on the high-resolution remote sensing database from 2003 to 2017. In general, the Kara Sea is fully covered with thicker sea ice in winter, but sea ice cover is continuously declining during the summer. The year 2003 was the year with the most severe ice conditions, while 2012 and 2016 were the least severe. The extensive sea ice begins to break up before May and becomes completely frozen at the end of December again. The duration of ice melting is approximately twice than that of the freezing. Since 2007, the minimum ice coverage has always been below 5%, resulting in wide open-waters in summer. Furthermore, the relevant local driving factors of external atmospheric forcing on ice conditions have been quantitatively calculated and analyzed. Winter accumulated surface air temperature has been playing a primary role on the ice concentration and thickness condition in winter and determining ice coverage index in the following melt-freeze stage. Correlation coefficients between winter accumulated temperature and ice thickness anomaly index, the ice coverage anomaly index, duration of melt-freeze stage can approach -0.72, -0.83 and 0.80, respectively. In summer, meridional winds contribute closely to summer ice coverage anomaly index, with correlation coefficient exceeding 0.80 since 2007 and 0.90 since 2010.

Key words: Arctic, ice regime, spatio-temporal variation, ice coverage anomaly index, atmospheric forcing factor, correlation analysis.

Introduction

Sea ice forms when seawater freezes and floats on the sea surface. In nearshore zones, the fast ice can expand even to several hundreds of kilometers, while in the offshore areas, the drift ice can sensitively move with strong winds and currents. Therefore, the extensive sea ice cover can trigger severe disasters, such

Copyright © 2019. Duan, Dong and Wang. This is an open-access article distributed under the terms of the Creative Commons Attribution-NonCommercial-NoDerivatives License (CC BY-NC-ND 3.0 https://creativecommons.org/licenses/by-nc-nd/3.0/), which permits use, distribution, and reproduction in any medium, provided that the article is properly cited, the use is non-commercial, and no modifications or adaptations are made.

as freezing wharves and ports, obstructing shipping route, threating navigation security, damaging marine structures, destructing oil and gas exploitation, destroying offshore platforms and submarine pipelines and affecting fisheries and aquaculture (Choi *et al*. 2015; Bergström *et al*. 2016).

As one of marginal seas of the Arctic Ocean, the Kara Sea, is an inevitable route of the Northeast Passage (Aksenov *et al*. 2017). The Kara Sea is connected to other marine basins and by land masses (Fig. 1). Northwards, it directly connects to the Arctic Ocean. Eastwards, it links to the Laptev Sea through the Severnaya Zemlya archipelago. Southwards, it is closely backed by Eurasia. Westwards, it is isolated from the Barents Sea by Novaya Zemlya and Kara Strait (International Hydrographic Organization 1953). In addition, the Kara Sea is abundant in oil and gas resources. According to the United States Geological Survey, the south Kara Sea contains 39%, 607 trillion cubic feet, of the potential gas resources on the Russian continental shelf regions (Gautier *et al*. 2009). Besides, the Kara Sea is also an important fishing ground, with about 77 different species of marine, freshwater and anadromous fish inhabiting the area (Dolgov 2013).

Thanks to the remote sensing satellite technology, the massive sea ice images of high resolution and quality gradually became available in the polar regions, which has already shown a shrinking and thinning trend for ice cover in the Arctic (Overland and Wang 2007; Lindsay and Schweiger 2015). The majority of studies focused on the physical mechanism between sea ice variations and thermodynamic and dynamical forcing, including warming sea surface temperature (Screen and Simmonds 2010), enhanced cyclone activities (Polyakov *et al*. 2003), and unsteady oceanic thermohaline circulation (Stroeve *et al*. 2007). But few studies have been devoted to separately analyze and quantify the recent ice regime in the Kara Sea. Instead, the nearby western Barents Sea has attracted the most attention to reveal its abnormal changes and governing factors (*e.g*., Sorteberg and Kvingedal 2006; Kwok 2009; Nakanowatari *et al*. 2014). With regard to Kara Sea, the characteristics of costal fast ice have been a focus in the existing research. Using observed measurements during 1953–2001, Divine

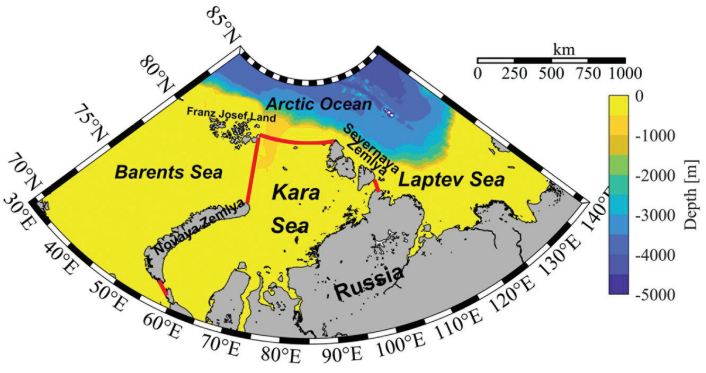

Fig. 1. Geographical and bathymetric map of the Kara Sea, with study area indicated.

et al. (2003, 2004, 2005) firstly described the temporal and spatial variations of fast ice, and the concomitant correlations with climatological factors and river runoff. Olason (2016) presented some modifications in the fundamental viscous–plastic dynamical equation and regarded the occurrence of static arching as the key step in fast ice freezing process in the Kara Sea. With respect to other relevant research, Belchansky *et al*. (1995) roughly computed the obvious ice cover retreat in the western Kara Sea from 1966 to 1983. However, in fact the sea extent of Kara Sea they defined indeed comprised the northeastern part of the Barents Sea. Kern *et al*. (2005) showed that accumulative ice volume export in winter from Kara Sea into Arctic Ocean could be totally up to 100–350 km^3 per year based on simulation results from 1996/97 to 2000/01. Cavalieri and Parkinson (2012) analyzed that the sea ice extent was decreasing with -9.2 ± 1.6% per decade in the Barents–Kara Sea during 1979–2010. Matishov *et al*. (2014) discovered that there was an abnormal ice distribution reduction in the Barents Sea and Kara Sea in winter months in 2012, which was perhaps as a result of atmospheric circulation blocking effect. Further, Ahn *et al*. (2014) utilized the ordinary least square regression to measure the interactions between ice concentration and climatic factors. Zhang *et al*. (2018) analyzed the lead-lag results of the stratospheric pathway in linking the mid-latitude atmospheric circulation to Barents–Kara Sea ice response based on a simplified statistical method. In addition, some studies focused on the effect of river runoff and inflowing Atlantic waters on the ice cover in the Kara Sea. The river runoff from Ob and Yenisei rivers provide an abundance of heat, which can accelerate the ice-melt near the estuaries (Harms and Karcher 1999; Hirche *et al*. 2006). The inflowing warm waters from North Atlantic, through northern seaway between Novaya Zemlya and Franz-Josef Land, can also play an important effect on ice cover conditions of Kara Sea by redistributing the heat in intermediate layer (Loeng *et al*. 1997; Schlichtholz 2013).

In some relevant Russian studies, Karklin *et al*. (2016) presented the changes in ice massifs areas of Kara Sea in the summer during the "cold" (1954–1985) and "warm" (1986–2017) climatic periods in the Arctic. Further, the ice patterns of ice stage development, drifting ice and fast ice in the autumn and winter during the above two climatic periods are described in southwest and northeast part of the Kara Sea, respectively (Karklin *et al*. 2017a, 2017b). According to aforementioned analysis, information on the recent sea ice condition variations in the Kara Sea is relatively inadequate and fragmentary to some extent. Therefore, it is of high value to better figure out the recent spatio-temporal variations of the ice regime in the Kara Sea and the relationship with the primary atmospheric influencing factors, such as sea surface air temperature and winds, in order to explain the local air–ice–ocean coupling interactions.

Thus, this paper is mainly aimed at characterizing the recent ice regime characteristics in the Kara Sea and the relationship with local atmospheric forcing

factors using the high-resolution sea ice remote sensing datasets available from 2003 to 2017. The paper is composed of four sections. The 'Materials and methods' section provides a description of the study area, remote sensing sea ice data, atmospheric data and some relevant approaches. 'Results and interpretations' section presents a detailed description on ice regime variability based on a set of evaluation indicators. 'Discussion' section attempts to give a quantitative explanation for linking ice regime to local atmospheric influencing variables. Finally, some brief relevant conclusions are summarized in 'Conclusions' section.

Materials and methods

Study area. — In this work, the whole study domain has been selected according to the defined limits of seas and oceans presented (Fig. 1; see also International Hydrographic Organization 1953). Specifically, the total Kara Sea is geographically situated within 66.5°N and has a total extent of roughly 8.8×10^6 km^2, with about 1 450 and 970 kilometers and 110 meters in length, width and average depth, respectively.

Sea ice concentration data. — We used the daily gridded sea ice concentration (SIC) dataset, the new sensor Advanced Microwave Scanning Radiometer-EOS and Radiometer 2 (AMSR-E and AMSR-2) data, obtained from the Institute of Environmental Physics in University of Bremen (Spreen *et al*. 2008). This retrieval sea ice data possesses the current highest horizontal resolution of 6.25 km × 6.25 km, which is nearly four times the resolution of the standard sensor Special Sensor Microwave/Imager (SSM/I). The database covers two periods, AMSR-E dataset during January 2003–October 2011 and AMSR-2 dataset during August 2012–December 2017. There is a blank period due to the abortion of AMSR-E. Herein, we have supplemented the missing sequences on the basis of the SSM/I database. The daily SSM/I ice concentration data can be available from the Integrated Climate Data Center (ICDC) in the University of Hamburg (http://icdc.cen.uni-hamburg.de/1/daten/cryosphere.html#c1694) and has spatial resolution of 12.5 km × 12.5 km with the polar stereographic projection, which is also four times the resolution of the conventional 25 km grid dataset from National Snow and Ice Data Center (https://nsidc.org/data/NSIDC-0051). Besides, it must be noted that the remote sensing AMSR ice data is more suitable to analyze climatic conditions (Spreen *et al*. 2008). Therefore, analysis described in this work is not for direct guiding ships for navigation purposes.

Sea ice thickness data. — Herein, the sea ice thickness data was also obtained from the ICDC (http://icdc.cen.uni-hamburg.de/1/daten/cryosphere.html#c1682; Tian-Kunze *et al*. 2016). Based on the European Space Agency Soil Moisture

and Ocean Salinity (SMOS) mission, the SMOS dataset has a complete daily coverage for polar regions and provides the ice thickness at a 12.5 km × 12.5 km grid using the same polar stereographic projection as above. It must be noted that ice thickness data sequence can so far be merely available in winter months from 2011 to 2017 due to larger retrieving deviation in summer.

Atmospheric forcing data. — External atmospheric factors data, including sea surface air temperature (SAT) at 2 m, winds velocity fields (including zonal and meridional vectors) at 10 m, were obtained from ERA-Interim reanalysis dataset of the European Centre for Medium-Range Weather Forecasts (ECMWF, www.apps.ecmwf.int/datasets/; Dee *et al*. 2011). The ERA-Interim dataset can well reflect atmospheric patterns in the Arctic (Kim *et al*. 2016). Both the daily SAT and winds data series, measured four times a day (0000 h, 0600 h, 1200 h and 1800 h), were chosen for the same period and at a spatial resolution of 1/8° × 1/8°.

Statistical methods. — All AMSR data is in HDF format and the other data are in NetCDF format. The statistical software MATLAB is a powerful tool to conduct the following analysis in this work. In order to describe the interannual ice regime in the Kara Sea, both the daily and monthly sea ice distributions, sea ice extent (*SIE*), and sea ice coverage (I_c) and other statistical parameters have been calculated based on the SIC dataset. The fundamental *SIE* is referred as the total extent of all grids more than 30% SIC. The I_c actually means the sea ice coverage rate in the total Kara Sea. Relevant formulas of *SIE* and I_c are computed as follows:

$$SIE = \int w_i s_i \mathrm{d}s \qquad \begin{cases} w_i = 1 & c_i \geq 30\% \\ w_i = 0 & c_i < 30\% \end{cases} \tag{1}$$

$$I_c = \frac{SIE}{S_k} \tag{2}$$

where c_i, s_i, and w_i represent the SIC, extent and weight coefficient in every grid in the whole domain, respectively, and the S_k represents the Kara Sea area. Other relevant defined statistical indicators judging ice conditions will be introduced and interpreted in different parts in 'Results and interpretations' section.

Furthermore, in order to determine and analyze the effect of local atmospheric indicators on the ice regime, relevance between atmospheric forcing and various regime statistical parameters have been calculated, which uses the *t*-test of p-value at 0.05. The correlation coefficient *R* can be given by following Eq. (3):

$$R = \frac{Cov(X,Y)}{\sqrt{Var(X)}\sqrt{Var(Y)}} \tag{3}$$

where *X* and *Y* represent the different ice regime statistical parameters. *Cov*(*X*,*Y*), *Var*(*X*) and *Var*(*Y*) represent the covariance and variance, respectively.

Results and interpretations

Monthly distributions of sea ice concentration. — It is significant to understand the temporal variation of ice occurrence in the Kara Sea. Therefore monthly mean spatial distributions of sea ice concentration have been averaged and drawn on the basis of the daily SIC sequences from 2003 to 2017.

The majority of sea ice in the Kara Sea belongs to first-year sea ice (Fig. 2). The formation and thaw have a regular annual cycle and a typical monthly variation in the whole study domain. Spatially, the SIC gradually becomes denser and denser from southwest to northeast. Temporally, from November to June, the whole sea area is entirely covered with substantial ice cover with different concentrations in different zones. The higher ice concentrations above 90% (even up to 100%) arise in the entire zone in winter and spring months. Besides, June and November are another two months with relatively serious ice regime. The former presents ice concentrations between 50% and 90%, while the latter is dominant by lower concentrations (< 50%) in the southwest and higher (> 70%) in the northeast. In July and October, an extensive ice-free zone occurs in the central and southwestern parts, but a medium concentration status (30–60%) still remains in the northeast. In August and September, most areas in the Kara Sea are exposed to the open waters and only a tiny residual lower concentration (< 30%) ice exists around the Seyernaya Zemlya Island.

Monthly distributions of sea ice thickness. — It is an integral part to visualize the temporal patterns of ice thickness in the Kara Sea. Hence, monthly mean spatial distributions of sea ice thickness have been computed and presented in terms of the daily ice thickness series in winter half year from 2010 to 2017.

The mean spatial distributions of ice thickness form October to April in the Kara Sea is shown on Fig. 3. Similar to the monthly concentrations patterns, the ice thickness also has a regular typical cycle and a substantial monthly variation in the entire research area. In spatial patterns, the ice thickness gradually increases from southwest to northeast. From January to April, the mean ice thickness is primarily between 40 and 80 cm in the southwest, and between 80 and 120 cm in the northeast. In November, the mean ice thickness is mainly between 20 and 60 cm in the most northeastern areas. In December, the average ice thickness is basically between 20 and 60 cm in the southwest, and between 60 and 100 cm in the northeast. The October is the month with the thinnest ice, less than 20 cm. In addition, we have calculated the maximum ice thickness in all grids in the study area from 2010 to 2017. All the grids have exceeded 100 cm thickness during these winters.

Characteristics of daily sea ice coverage and melt-freeze period. — Sea ice coverage is an effective statistical indicator to describe ice regime variations in the Kara Sea. Using the SIC series dataset, the daily *SIE* and I_c in Kara Sea

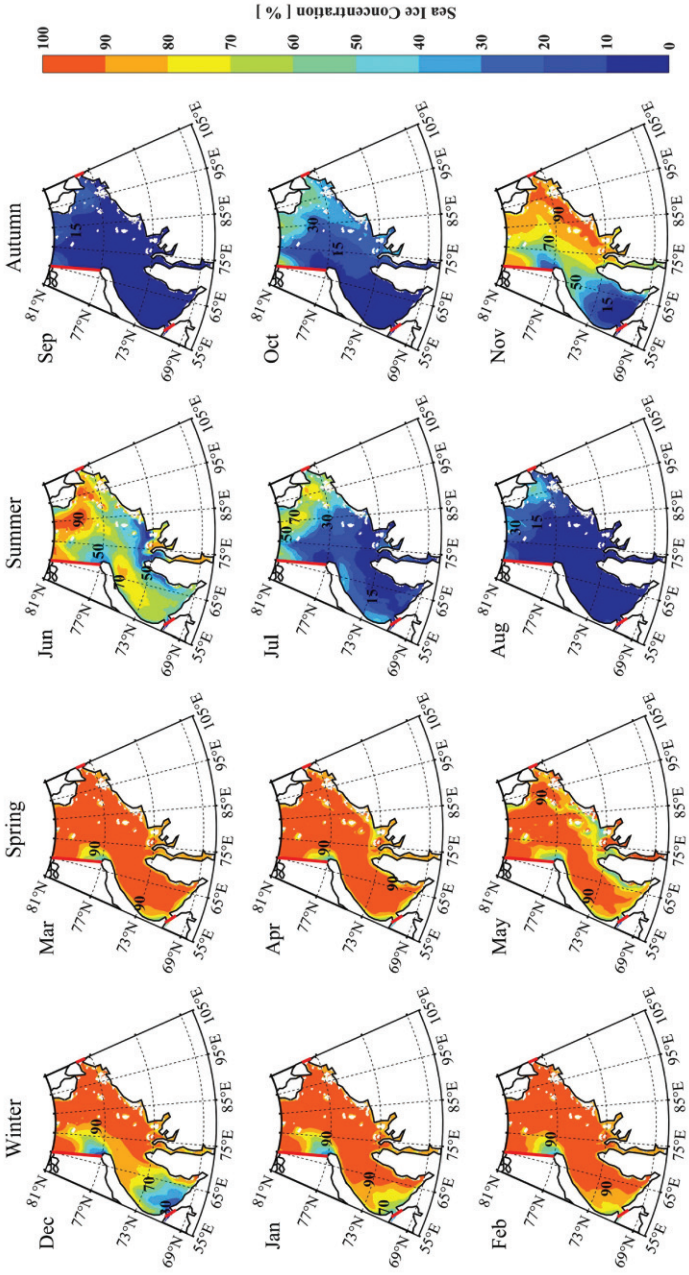

Fig. 2. Distributions of monthly mean sea ice concentration in the Kara Sea from winter to autumn during 2003–2017.

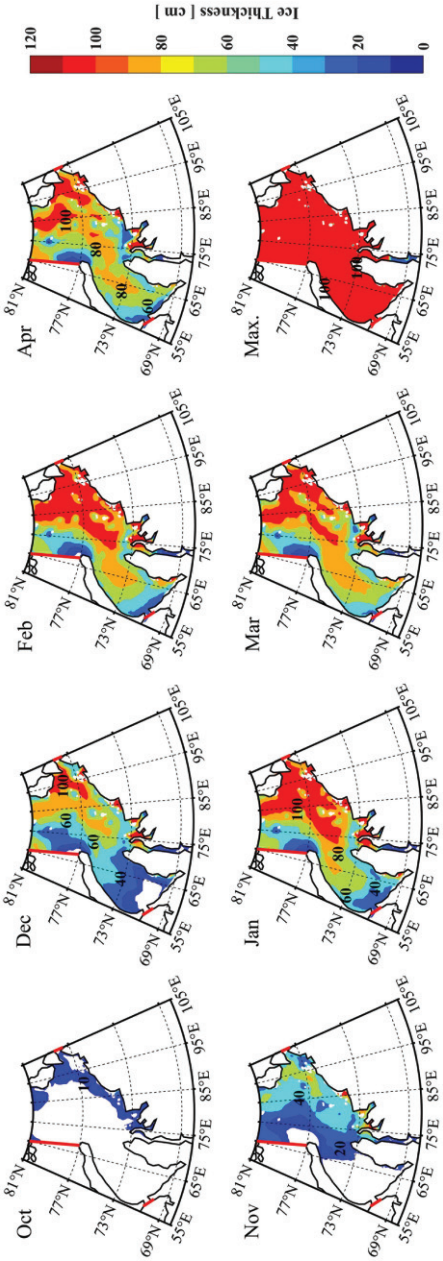

Fig. 3. Distributions of the monthly mean sea ice thickness in the Kara Sea from October to April during 2003–2017 and the maximum ice thickness (in cm).

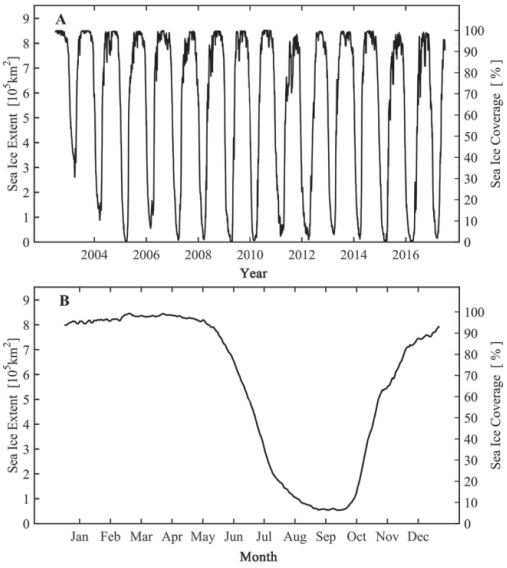

Fig. 4. Interannual variations of daily ice coverage and sea ice extent (**A**) and multiyear daily average values (**B**) in the Kara Sea during 2003–2017.

have been presented from 2003 to 2017, successively. Based on the Eq. (1–2), daily variations of *SIE* and I_c, and the multiyear average daily results have been plotted in Fig. 4.

Several sea ice features can be inferred in the Kara Sea (Fig. 4) First of all, in winter months the Kara Sea is fully covered with ice cover, though with occasional minor fluctuations. Then we have concentrated on melt-freeze period in the Kara Sea, during which sea ice begins to break up in spring and fully freeze in winter. In general, the whole domain starts to melt in May and completely freezes by the end of December. Concretely, the duration of ice melting stage is comparatively slower than that of freezing stage. The melting process approximately takes place from May to September (4–5 months), while the freezing process sustains from October to December (2–3 months). Further, during the melting process, the initial and final periods are relatively smooth, with a mean monthly sea ice coverage loss about 10%, but the middle period varies greatly, with a 60% ice coverage reduction. During the freezing process, October rises tremendously with a total 50% ice coverage increase, and the following months only increase about 30%. In addition, the mean smallest I_c occurs in September. Particularly, the smallest coverage has spectacular interannual variations from 2003 to 2017 (Fig. 5). The year 2003 and 2004 have the highest values. But since 2007, the lowest coverage has been less than 5% continuously, meaning that the extensive open-water forms in the summer.

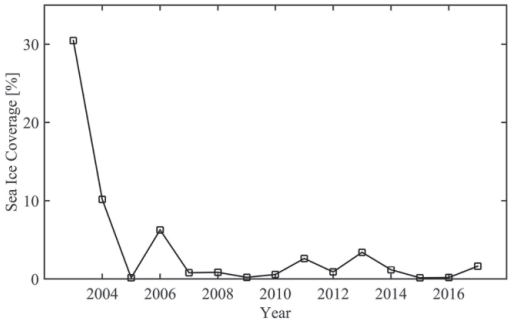

Fig. 5. Interannual variations of the minimum daily ice coverage in the Kara Sea during 2003–2017.

Interannual variations of daily sea ice coverage anomaly. — Based on the daily ice coverage sequences, the interannual sea ice coverage anomaly series I_d have been calculated from 2003 to 2017. Herein, the positive anomaly phases with larger absolute values represent heavy ice regime, the negative anomaly ones with larger absolute values represent light ice regime, and other phases with smaller absolute values represent medium ice regime. The I_d is given by:

$$I_d = I'_{n,m} = I_{n,m} - \overline{I}_n \tag{4}$$

where I_d, $I_{n,m}$ and $\overline{I}_n$ are the daily ice coverage anomaly index in m-th year, ice coverage in n-th day of m-th year and multi-year mean ice coverage in n-th day, respectively.

The I_d is undergoing a tendency from positive phases to negative ones from 2003 to 2017 (Fig. 6). It means that ice regime in the Kara Sea is gradually becoming lighter in recent years. In particular, year 2003 performs the heaviest ice condition with a noticeable anomaly peak (even up to 40%) in summer months. The special abnormal phenomenon might be induced by the enormous ice volume import from the Arctic Ocean (Deser and Teng 2008). Besides, the years 2004–2006 and 2014 can be treated as another four heavier ice regime typical cases. Regarding the medium ice conditions, years 2007–2010 and 2013 can be regarded as typical examples. In these years, the ice coverage anomaly phases feature with a sign-alternating case. Furthermore, years 2012 and 2016 are the lightest ice regime years, with several remarkable negative anomaly phases in winter months. In 2012, the coverage anomaly can be up to -20% and -40% during January and November. In 2016, the coverage anomaly is even less than -50% during November. Other years, such as 2011, 2015 and 2017, are also the lighter ice regime years.

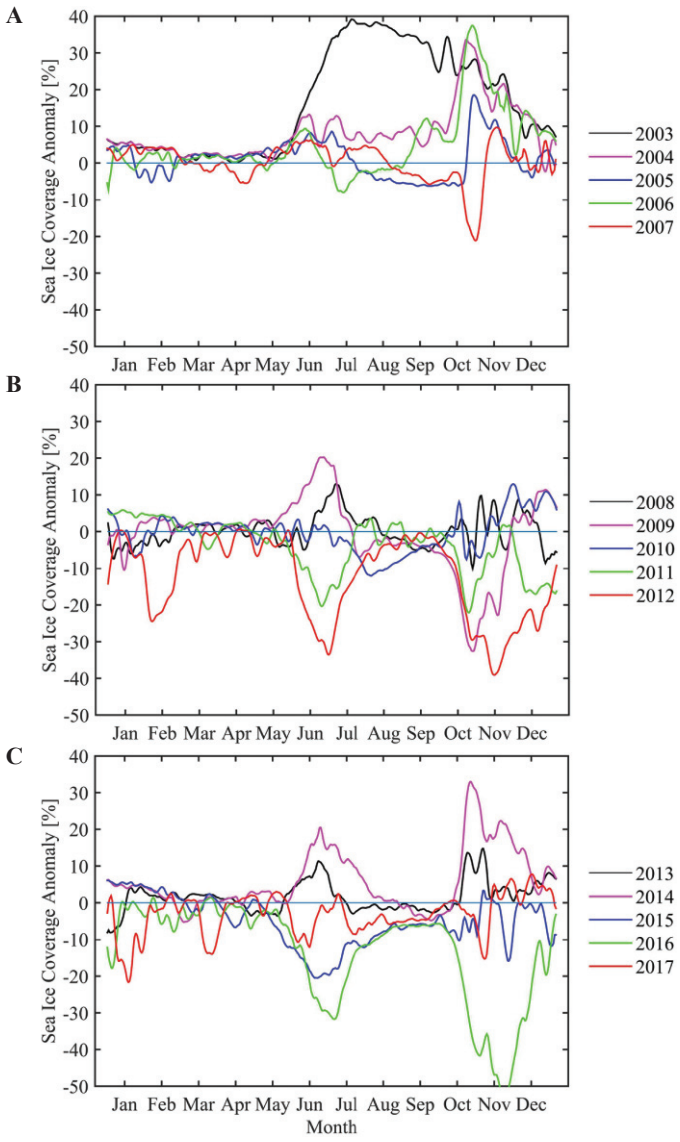

Fig. 6. Interannual variations of the daily ice coverage anomaly in the Kara Sea during 2003–2007 (**A**), 2008–2012 (**B**) and 2013–2017 (**C**).

Interannual variations of melt-freeze period and growth period. — Two statistical parameters are introduced to quantify ice regime in the melt–freeze period in the Kara Sea. The first one is named as melt–freeze sea ice coverage anomaly index I_m, which is practically equal to the mean ice coverage anomaly in a certain period. On the basis of daily ice coverage I_d characteristics (Fig. 4), the period from May 1st to December 31st, when the ice coverage shows

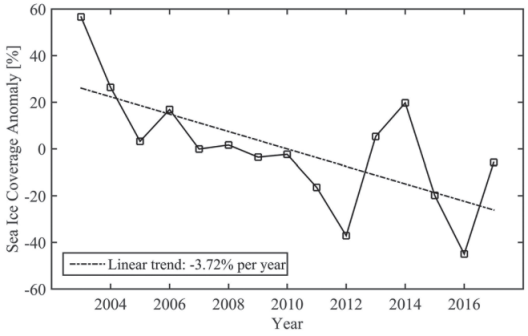

Fig. 7. Interannual variations of the melt-freeze sea ice coverage anomaly index in the Kara Sea during 2003–2017.

a prominent variation, is chosen as the time interval to calculate this index I_m (Fig. 7). The larger the I_m is, the heavier the ice regime is. The equation is given by:

$$I_m = \frac{1}{245} \sum_{n=121}^{365} \left(I_{n,m} - \bar{I}_n \right) \tag{5}$$

where $I_{n,m}$ and $\bar{I}_n$ are defined the same as in Eq. 4. The second statistical parameter is defined as the duration of melt-freeze period L. It is the length of period (number of days) from beginning of ice melt/thaw till beginning of fully frozen condition in the Kara Sea. The longer the L is, the lighter the ice condition is. The formula of L is expressed as:

$$L = D_f - D_m \tag{6}$$

where L, D_f and D_m are the duration of melt-freeze period, the final day and initial day when sea ice coverage in the Kara Sea approaches 90% for the first time in the freezing stage and last time in the melting stage, respectively.

On the basis of preceding I_d results, the interannual variations of melt-freeze ice coverage anomaly index I_m from 2003 to 2017 can be inferred (Fig. 7). Generally, the I_m shows a downward trend. Year 2003 possesses the largest I_m value (56.6%), meaning 2003 is the heaviest ice status in melt-freeze period during 2003–2017. Besides, years 2004–2006, 2013–2014 also have relatively larger values. In contrast, years 2016 and 2012 have the two lowest I_m values (-45.0% and -37.1%, respectively), demonstrating the lightest ice situation in recent years. More details of interannual variation of melt-freeze period, including the duration, initial day and final day are presented on Fig. 8. As is shown, the final day of melt-freeze period basically distributes in October and November, but the associated initial day occurs earlier and earlier year by year during

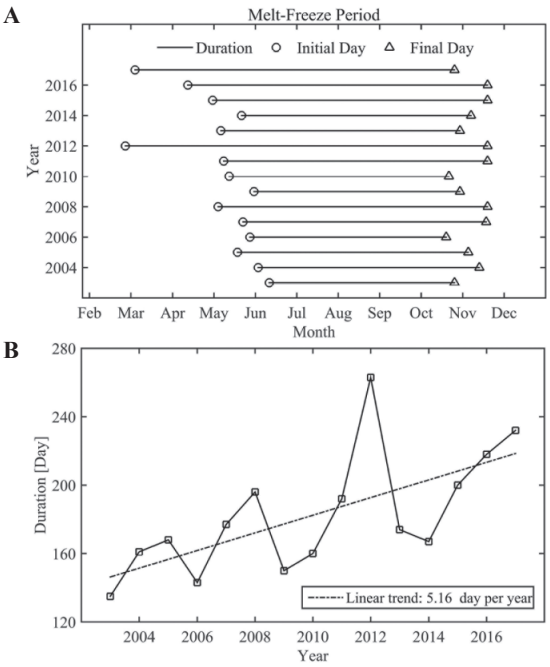

Fig. 8. Interannual variations of the melt-freeze period (**A**) and its duration (**B**) during 2003–2017.

2003–2017. Therefore, the L duration gradually becomes longer and longer, from 135 d in 2003 to 263 d in 2012 and 218 d in 2017, though with some uncertain oscillations. Year 2012 has the longest duration and earliest initial day while 2003 is the exactly opposite. This striking contrast is well consistent with preceding ice status analysis of daily sea ice coverage anomaly. Further, the I_m and L are in good relevance with the correlation coefficient -0.78 (at significance at 95% confidence level).

As for the sea ice growth period, the ice thickness anomaly index H_m is firstly presented and defined to characterize the ice conditions during 2011–2017. In details, the space average ice thickness from October (last year) to April (this year) is considered as the H_m. The equations are given by:

$$H_m = \frac{1}{183}\left[\sum_{n=288}^{365}\left(H_{n,m} - \bar{H}_n\right) + \sum_{n=1}^{105}\left(H_{n,m} - \bar{H}_n\right)\right] \tag{7}$$

$$H = \frac{1}{S_K}\int w_i s_i c_i h_i \mathrm{d}s \qquad \begin{cases} w_i = 1 & c_i \geq 30\% \\ w_i = 0 & c_i < 30\% \end{cases} \tag{8}$$

where H_m, $H_{n,m}$ and $\bar{H}_n$ denote the ice thickness anomaly index m-th year, ice thickness in n-th day of m-th year and multi-year mean ice thickness in n-th day, respectively.

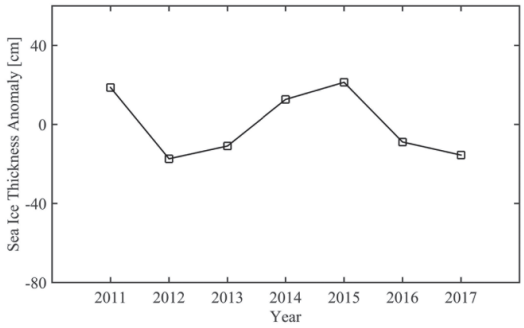

Fig. 9. Interannual variations of winter sea ice thickness anomaly index in the Kara Sea during 2011–2017.

The interannual variations of H_m from 2011 to 2017 are shown on Fig. 9. Years 2012, 2013, 2015 and 2016 have the lower anomaly phases while 2011, 2014 and 2015 have the higher ones. The positive and negative oscillation is visible.

Discussion

Based on the above climatic ice regime analysis, it may be inferred that sea ice in the Kara Sea has decreased in summer months, which well conforms to the sea ice overall change in the entire Arctic (Serreze *et al*. 2007). Specifically, Divine *et al*. (2004) calculated the appearance frequency of fast ice using Russian observations during 1953–1990, and their findings are relatively higher than SIC values in this work in summer months. Thus in the following content, we discuss the effects of the local atmospheric factors on the sea ice regime variations.

Relation between winter accumulated temperature and ice regime. — Air temperature has been increasing in the Arctic. Thus, it is prerequisite to identify the relevance between sea surface air temperature (SAT) and ice situation in the Kara Sea. In general, the effect of SAT on sea ice is a comparatively gradual accumulation process. The winter accumulated temperature T_a is an effective test statistic. T_a has an irreplaceable influence on sea ice formation and thaw, which can determine the ice condition in the following melt-freeze period (Wang and Ikeda 2000). In this study, duration from November (last year) to April (this year) is selected as the integral interval to obtain the T_a in the Kara Sea. The formula for estimating T_a is expressed as:

$$T_a = \frac{1}{T_t \bullet S_k} \iint T(s,t)\,\mathrm{d}s\,\mathrm{d}t \tag{9}$$

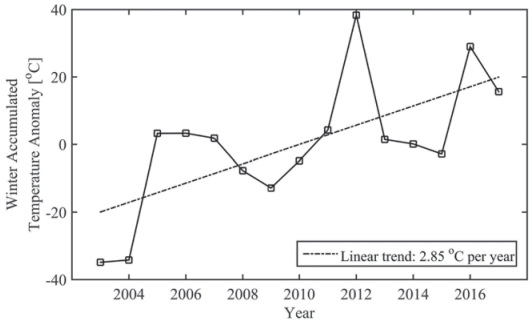

Fig. 10. Interannual variations of winter accumulated temperature anomaly in the Kara Sea during 2003–2017.

where $T(s,t)$ and T_t denote the accumulated temperature per unit area and time, and the total time, respectively.

Based on the daily ECMWF ERA-Interim SAT series, the T_a has been estimated from 2003 to 2017, continuously. In spite of some unsteady fluctuations, the T_a anomaly shows an apparent upward trend and transforms from negative anomaly phases into positive ones (Fig. 10). It should be noted that once the T_a significantly increases, the ice concentrations decrease, otherwise, the ice condition turns into the opposite. Table 1 has clearly interpreted correlation coefficients during 2003–2017 between T_a and the previous various ice regime statistical indicators, including the melt-freeze sea ice coverage anomaly index I_m, the annual minimum I_c, the duration of melt-freeze period L and its initial day, and ice thickness anomaly index H_m.

Table 1

Correlation coefficients (R) between winter accumulated temperature (T_a) and melt-freeze sea ice coverage anomaly index (I_m), minimum ice coverage (I_c), duration of melt-freeze period (L) and its initial day, and ice thickness anomaly index H_m in the Kara Sea (significance at 95% confidence level).

R	T_a	I_m	Min. I_c	L	Initial day of L	H_m
T_a	1	–0.83	–0.62	0.80	0.81	–0.72
I_m	–0.83	1	0.75	–0.78	0.69	–
Min. I_c	–0.62	0.75	1	–0.46	–	–
L	0.80	–0.78	–0.46	1	0.94	–
Initial day of L	0.81	0.69	–	–0.94	1	–
H_m	–0.72	–	–	–	–	1

The T_a parameter is highly correlated with above indicators, with -0.83, -0.62, 0.80, -0.81 and -0.72 (significance at 95% confidence level), respectively (Table 1). In particular, for the heaviest ice regime year, in 2003 the T_a is at its lowest peak (-34.9°C), in the meantime, the I_m and minimum I_c are also at their highest peaks, and the L and its initial day are at their lowest locations as well. For the lightest ice condition year, in 2012 the T_a is at the abrupt sharp peak (38.3°C), accordingly, the I_m and minimum I_c are also at their lower peaks, and the L and its initial day are at their largest positions as well. Besides, in this year, a negative ice coverage occurs in February (Fig. 6), which can be reasonably explained by the positive highest T_a anomaly. Specifically, Matishov *et al*. (2014) believed that the ice loss in 2012 in the Kara Sea is perhaps caused by the abnormal atmospheric circulation blocking incident. Therefore, it can deduce that the winter accumulated temperature T_a can effectively determine the ice regime in the Kara Sea. Further, with the increasing T_a, sea ice is simultaneously undergoing a transition from heavier status to lighter conditions, especially in summer months.

Relation between summer wind fields and ice condition. — In sea ice marginal zones, the ice motion is sensitively carried by the strong sea surface winds, and consequently ice coverage can vary abruptly in a short period, which can perhaps jeopardize offshore activities. Therefore on the basis of the ECMWF ERA-Interim reanalysis dataset, average monthly winds in the Kara Sea, including zonal U and meridional V indexes, from 2003 to 2017 have been estimated based on the space mean approach. The relevant equations are expressed as:

$$U = \frac{1}{T_t \bullet S_k} \iint u(s,t)\mathrm{d}s\mathrm{d}t \tag{10}$$

$$V = \frac{1}{T_t \bullet S_k} \iint v(s,t)\mathrm{d}s\mathrm{d}t \tag{11}$$

where u and v represent the speed vectors in every grid. Herein the direction is where wind blows from.

Since the Kara Sea is geographically semi-enclosed, sea ice migration in zonal directions is usually blocked by islands and land but has a better response to the winds in meridional directions. The interannual variations of wind vector fields in the Kara Sea from 2003 to 2017 are shown on Fig. 11. The southerly winds are comparatively prevailing in summer months, indicating it is favorable to impede the cold air from higher latitudes but promote warm air from the Eurasian into the Kara Sea. In addition, the dominant southerly winds can reduce the ice volume import from Arctic Ocean as well, which is consistent with the previous results by Pfirman *et al*. (1997). In all, these factors can favor a lighter ice situation in summer months.

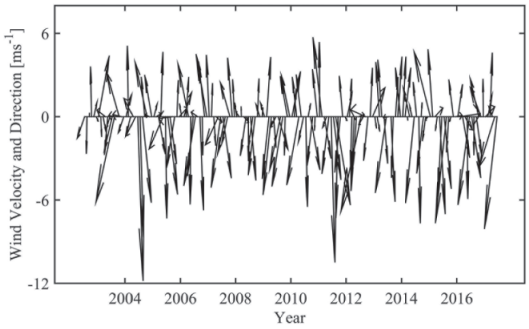

Fig. 11. Interannual variations of mean wind vector fields in the Kara Sea during 2003–2017. The positive phase of *x*-axis (*U*) and *y*-axis (*V*) denote the westerly and southerly winds, respectively.

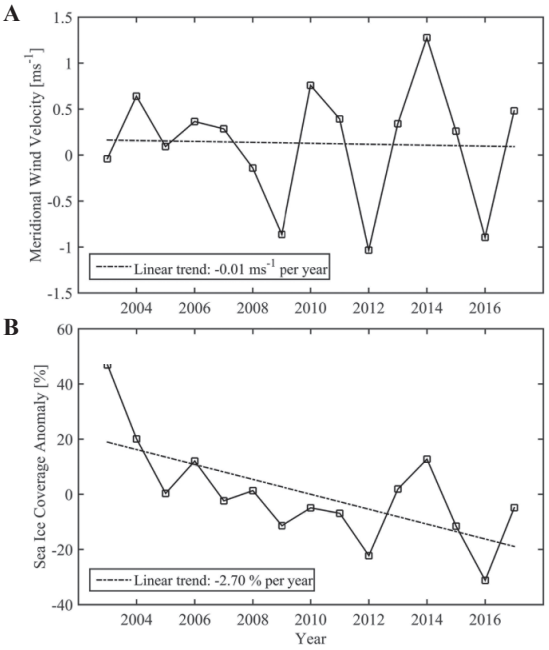

Fig. 12. Interannual variations of meridional wind fields (**A**) and the simultaneous summer ice coverage anomaly index (**B**) during 2003–2017.

Further, we have analyzed the mean meridional wind index and the synchronous summer sea ice coverage anomaly index from June to November, during which the ice coverage is quite low in the annual cycle. In 15 years in total, the two indexes are in good relevance (Fig. 12). Especially, since 2003 (*i.e.* from 2003 to 2017), the correlation coefficient can approach 0.49; since 2004, coefficient can exceed 0.70; since 2007, coefficient can approach 0.80; and since 2011, coefficient can approach 0.90 (Table 2). Thus it can be inferred

Table 2

Correlation coefficients (R) between summer meridional wind index and the simultaneous ice coverage anomaly index since different initial years (significance at 95% confidence level).

Initial year	2003	2004	2005	2006	2007
R	0.49	0.76	0.77	0.77	0.81
Initial year	2008	2009	2010	2011	2012
R	0.81	0.86	0.86	0.93	0.94

that the meridional winds can also impact the summer sea ice distributions in the Kara Sea. This deduction can also conform to the assumption that sea ice movement can fundamentally response well with wind states when ice coverage is in lower situations (Martin and Wadhams 1999).

Conclusions

This investigation has presented a statistical description of the recent ice regime characteristics in the Kara Sea and its interactions with local atmospheric factors using higher resolution remote sensing sea ice database and ECMWF ERA-Interim reanalysis dataset from 2003 to 2017. Several characteristics can be given:

1. Sea ice distributions have an obvious variability both seasonally and interannually in the Kara Sea. 2003 is the heaviest ice regime year, while 2012 and 2016 are lightest ones. The whole sea is completely covered with a higher concentration and a thicker sea ice in winter, but a continuous ice decrease occurs in summer. Since 2007, the lowest ice coverage has been nearly 5%, meaning the extensive open-water occurrence in summer.
2. The duration of ice melting period is approximately twice than that of freezing period. The length of melt-freeze period gradually has become longer than before, with the initial day occurring earlier every year. The melt–freeze sea ice coverage anomaly index is undergoing a transition from positive to negative phases during 2003–2017. All the statistical indicators show that the ice regime in the Kara Sea is gradually becoming lighter in recent years.
3. Ice regime is closely sensitive to sea surface air temperature. Winter accumulated temperature can significantly determine the ice regime during the ice growth period and also in the following melt–freeze period. The accumulated temperature can well explain the abnormal regime years, such as

the heaviest year 2003, and the lightest years 2012 and 2016. High correlations are maintained between accumulated temperature and ice thickness anomaly index, ice coverage anomaly index, duration of melt–freeze stage.

4. Since 2004, the summer sea ice anomaly index becomes closely related to the meridional winds in the Kara Sea with correlation of about 0.72. In particular, the correlation coefficient gradually becomes enhanced in the following years. Besides, the predominant southerly winds are capable to reduce ice conditions in the summer.

In summary, the ice regime in the Kara Sea is undergoing a transition from heavier status to lighter conditions, and it is vulnerably affected by abrupt and abnormal sea surface air temperature and wind fields. Further work is required when more observable measurements are available in order to gain insight into other aspects of sea ice regime, such as drifting behaviors.

Acknowledgements. — The anthors are greatly thankful to the reviewers Anna Bulczak, Denis Moiseev and Tadeusz Pastusiak for their valuable suggestions. This work is financially supported by the National Natural Science Foundation of China (No. 51779236 and 51509226).

References

AHN J., HONG S., CHO J., LEE Y.W. and LEE H. 2014. Statistical modeling of sea ice concentration using satellite imagery and climate reanalysis data in the Barents and Kara seas, 1979–2012. *Remote Sensing* 6: 5520–5540.

AKSENOV Y., POPOVA E.E., YOOL A., NURSER A.J.G., WILLIAMS T.D., BERTINO L. and BERGH J. 2017. On the future navigability of arctic sea routes: high-resolution projections of the Arctic Ocean and sea ice. *Marine Policy* 75: 300–317.

BELCHANSKY G.I., MORDVINTSEV I.N., OVCHINNIKOV G.K. and DOUGLAS D.C. 1995. Assessing trends in Arctic sea-ice distribution in the Barents and Kara seas using the Kosmos–Okean satellite series. *Polar Record* 31: 129–134.

BERGSTRÖM M., ERIKSTAD S.O. and EHLERS S. 2016. Assessment of the applicability of goal-and risk-based design on Arctic sea transport systems. *Ocean Engineering* 128: 183–198.

CAVALIERI D.J. and PARKINSON C.L. 2012. Arctic sea ice variability and trends, 1979–2010. *The Cryosphere* 6: 881–889.

CHOI M., CHUNG H., YAMAGUCHI H. and NAGAKAWA K. 2015. Arctic sea route path planning based on an uncertain ice prediction model. *Cold Regions Science and Technology* 109: 61–69.

DEE D.P., UPPALA S.M., SIMMONS A.J., BERRISFORD P., POLI P., KOBAYASHI S., ANDRAE U., BALMASEDA M.A., BALSAMO G., BAUER P., BECHTOLD P., BELJAARS A.C.M., VAN DE BERG L., BIDLOT J., BORMANN N., DELSOL C., DRAGANI R., FUENTES M., GEER A.J., HAIMBERGER L., HEALY S.B., HERSBACH H., HÓLM E.V., ISAKSEN L., KÅLLBERG P., KÖHLER M., MATRICARDI M., MCNALLY A.P., MONGE-SANZ B.M., PARK B.-K., PEUBEY C., DE ROSNAY P, TAVOLATO C., THÉPAUT J.-N. and VITART F. 2011. The ERA-Interim reanalysis: configuration and performance of the data assimilation system. *Quarterly Journal of the Royal Meteorological Society* 137: 553–597.

DESER C. and TENG H. 2008. Evolution of Arctic sea ice concentration trends and the role of atmospheric circulation forcing, 1979–2007. *Geophysical Research Letters* 35, L02504.

DIVINE D.V., KORSNES R. and MAKSHTAS A. 2003. Variability and climate sensitivity of fast ice extent in the north-eastern Kara Sea. *Polar Research* 22: 27–34.

DIVINE D.V., KORSNES R. and MAKSHTAS A.P. 2004. Temporal and spatial variation of shore-fast ice in the Kara Sea. *Continental Shelf Research* 24: 1717–1736.

DIVINE D.V., KORSNES R., MAKSHTAS A.P., GODTLIEBSEN F. and SVENDSEN H. 2005. Atmospheric-driven state transfer of shore-fast ice in the northeastern Kara Sea. *Journal of Geophysical Research: Oceans* 110: C09013.

DOLGOV A.V. 2013. Annotated list of fish-like vertebrates and fish of the Kara Sea. *Journal of Ichthyology* 53: 914–922.

GAUTIER D.L., BIRD K.J., CHARPENTIER R.R., GRANTZ A., HOUSEKNECHT D.W., KLETT T.R., MOORE T.E., PITMAN J.K., SCHENK J., SCHUENEMEYER J.H., SØRENSEN K., TENNYSON M.E., VALIN Z.C. and WANDREY C.J. 2009. Assessment of undiscovered oil and gas in the Arctic. *Science* 324: 1175–1179.

HARMS I.H. and KARCHER M.J. 1999. Modeling the seasonal variability of hydrography and circulation in the Kara Sea. *Journal of Geophysical Research: Oceans*, 104: 13431–13448.

HIRCHE H.J., KOSOBOKOVA K.N., GAYE-HAAKE B., HARMS I., MEON B. and NÖTHIG E.M. 2006. Structure and function of contemporary food webs on Arctic shelves: A panarctic comparison: The pelagic system of the Kara Sea–Communities and components of carbon flow. *Progress in Oceanography* 71: 288–313.

INTERNATIONAL HYDROGRAPHIC ORGANIZATION. 1953. *Limits of oceans and seas* (No. 23). International Hydrographic Organization: 8 pp.

LOENG H., OZHIGIN V. and ÅDLANDSVIK B. 1997. Water fluxes through the Barents Sea. *ICES Journal of Marine Science* 54: 310–317.

KARKLIN V.P., HOTCHENKOV S.V., YULIN A.V. and SMOLYANITSKY V.M. 2016. Seasonal changes in the stages of sea ice development in northeast part of the Kara Sea during the autumn and winter period. *Arctic and Antarctic Research* 4: 41–50. (In Russian).

KARKLIN V.P., HOTCHENKOV S.V., YULIN A.V. and SMOLYANITSKY V.M. 2017a. Formation of the stages of sea ice development composition in the south-western part of the Kara Sea during autumn-winter season. *Arctic and Antarctic Research* 3: 16–26. (In Russian).

KARKLIN V.P., YULIN A.V., SHARATUNOVA M.V. and MOCHNOVA L.P. 2017b. Climate variability of the Kara Sea ice massifs. *Arctic and Antarctic Research* 4: 37–46. (In Russian).

KERN S., HARMS I., BAKAN S. and CHEN Y. 2005. A comprehensive view of Kara Sea polynya dynamics, sea-ice compactness and export from model and remote sensing data. *Geophysical Research Letters* 32: L15501.

KWOK R. 2009. Outflow of Arctic Ocean sea ice into the Greenland and Barents Seas: 1979–2007. *Journal of Climate* 22: 2438–2457.

KIM K.Y., HAMLINGTON B.D., NA H. and KIM J. 2016. Mechanism of seasonal Arctic sea ice evolution and Arctic amplification. *The Cryosphere* 10: 2191–2202.

LINDSAY R. and SCHWEIGER A. 2015. Arctic sea ice thickness loss determined using subsurface, aircraft, and satellite observations. *The Cryosphere* 9: 269–283.

MARTIN T. and WADHAMS P. 1999. Sea-ice flux in the East Greenland Current. *Deep Sea Research Part II: Topical Studies in Oceanography* 46: 1063–1082.

MATISHOV G.G., DZHENYUK S.L., MOISEEV D.V. and ZHICHKIN A.P. 2014. Pronounced anomalies of air, water, ice conditions in the Barents and Kara Seas, and the Sea of Azov. *Oceanologia* 56: 445–460.

NAKANOWATARI T., SATO K. and INOUE J. 2014. Predictability of the Barents Sea ice in early winter: Remote effects of oceanic and atmospheric thermal conditions from the North Atlantic. *Journal of Climate* 27: 8884–8901.

OLASON E. 2016. A dynamical model of Kara Sea land-fast ice. *Journal of Geophysical Research: Oceans* 121: 3141–3158.

OVERLAND J.E. and WANG M. 2007. Future regional Arctic sea ice declines. *Geophysical Research Letters* 34: L17705.

PFIRMAN S.L., KÖGELER J.W. and RIGOR I. 1997. Potential for rapid transport of contaminants from the Kara Sea. *Science of the Total Environment* 202: 111–122.

POLYAKOV I.V., ALEKSEEV G.V., BEKRYAEV R.V., BHATT U.S., COLONY R., JOHNSON M.A., KARKLIN V.P., WALSH D. and YULIN A.V. 2003. Long-term ice variability in Arctic marginal seas. *Journal of Climate* 16: 2078–2085.

SCHLICHTHOLZ P. 2013. Observational evidence for oceanic forcing of atmospheric variability in the Nordic seas area. *Journal of Climate* 26: 2957–2975.

SCREEN J.A. and SIMMONDS I. 2010. The central role of diminishing sea ice in recent Arctic temperature amplification. *Nature* 464: 1334–1337

SERREZE M.C., HOLLAND M.M. and STROEVE J. 2007. Perspectives on the Arctic's shrinking sea ice cover. *Science* 315: 1533–1536.

SORTEBERG A. and KVINGEDAL B. 2006. Atmospheric forcing on the Barents Sea winter ice extent. *Journal of Climate* 19: 4772–4784.

SPREEN G., KALESCHKE L. and HEYGSTER G. 2008. Sea ice remote sensing using AMSR-E 89-GHz channels. *Journal of Geophysical Research: Oceans* 113: C02S03.

STROEVE J., HOLLAND M.M., MEIER W., SCAMBOS T. and SERREZE M 2007. Arctic sea ice decline: Faster than forecast. *Geophysical Research Letters* 34: L09501.

TIAN-KUNZE X., KALESCHKE L. and MAASS N. 2016. *SMOS Daily sea ice thickness version 3*, ICDC, University of Hamburg, Germany.

WANG J. and IKEDA M. 2000. Arctic oscillation and Arctic sea-ice oscillation. *Geophysical Research Letters* 27: 1287–1290.

ZHANG P., WU Y. and SMITH K.L. 2018. Prolonged effect of the stratospheric pathway in linking Barents–Kara Sea sea ice variability to the midlatitude circulation in a simplified model. *Climate Dynamics* 50: 527–539.

Received 12 December 2018
Accepted 28 June 2019